

AN IMPROVED DESTRIPIING METHOD FOR REMOTE SENSING IMAGES

Zhiping Dan,^{*,**} Xing Wei,^{*,**} Shuifa Sun,^{*,**} and Gang Zhou^{***}

Abstract

Aiming at the problem of the stripe noises of agricultural remote sensing (RS) images, an improved destripping method high order unidirectional total variation with split-bregman iteration (HOUTV-SBI) for agricultural RS images is proposed by a higher-order partial differential model. The new method is based on the unidirectional total variation (UTV) model. It could highly performance remove the stripe noises, and effectively suppress the “ripple phenomenon” followed by UTV model. The experiments are compared with other traditional algorithms on the satellite images and their simulation images with two kinds of imaging systems. The results show that our method has good adaptability for removing all kinds of periodic and non-periodic random stripe noises and could provide better practicability.

Key Words

Agricultural application, stripe noise, higher-order partial differential, unidirectional total variation, Split-Bregman

1. Introduction

Remote sensing (RS) images are used in many applications [1] such as agricultural monitoring, disaster prevention, environmental protection. However, stripe noises are widely existed in various imaging systems such as spaceborne imaging systems, airborne spectrometer imaging systems, and so on. Because of the non-linear response of imaging units or the influence of bad pixels, the image data will appear as the grey value of continuous high or low in a certain direction and form the line of stripe noise easily in the push broom imaging equipment. The noise covers the real information of radiation in the image, reduces the quality of the image, and affects seriously for the subsequent process of feature extracted and target recognition,

* Hubei Key Laboratory of Intelligent Vision Based Monitoring for Hydroelectric Engineering, China Three Gorges University, Yichang 443002, China; e-mail: zp_dan@ctgu.edu.cn, 2440118749@qq.com, 183089433@qq.com

** Collaborative Innovation Center for Geo-Hazards and Eco-Environment in Three Gorges Area, Hubei province, Yichang 443002, China

*** School of Automation, Huazhong University of Science and Technology, Wuhan 430074, China; e-mail: 254530371@qq.com
Corresponding author: Shuifa Sun

Recommended by Prof. Simon X. Yang
(DOI: 10.2316/Journal.206.2018.1.206-5549)

etc. Therefore, it is necessary to suppress and eliminate this kind of noise.

The current camera can suppress the noise in small range by using the prelaunch and in-flight radiation calibration [2], while it still cannot completely eliminate stripe noise. At present, there are mainly three kinds of methods to eliminate the stripe noise. The first class method is based on the histogram matching method [3] and moment matching method [4]. It normalizes image’s grey information itself and chooses a detection unit as a reference in each band, and then the grey value distribution of other detection units can be adjusted by using those referred to eliminate the stripe noise. The second class method is based on transform domain method, the main representative of which are the Fourier transform [5] and the wavelet domain transformation [6]. The common characteristic of this class method is that it assumes that stripe noise only exists in a certain frequencies after the image transformed. According to the corresponding inverse transformation, the method can achieve the goal of suppressing stripe noise for low-pass filtering in certain frequencies. The third class method is based on the partial differential equation [7], which establishes the unidirectional total variation (UTV) model based on the direction feature of the stripe noise. Finally, the stripe noise problem is converted into energy functional minimization problem. In recent years, the eliminations of stripe noises have been paid more attention of researchers especially for hyperspectral data [8] and moderator resolution imaging spectrometer (MODIS) data [9], especially based on the variation model. Though the variation model has achieved good results, because of the characteristics of the total variation, it is easy to cause the “ripple phenomenon” [10]. To solve this problem, a higher-order partial differential algorithm model is proposed based on the UTV model and Split-Bregman iteration. In experiments, the proposed method not only can retain advantages of UTV model but also can effectively eliminate the “ripple phenomenon”.

2. Destripping Method Description

We assume that the stripe noise is an additive noise, and then the degradation process of RS images can be described as:

$$g = u + n \quad (1)$$

where g is degraded image, u is latent image to be restored, and n is the stripe noise.

Marouan Bouali exploited the scan line noise had a unidirectional property which was incorporated on UTV framework [7]. In the framework, destriping can be regarded as an optimization problem, and it can be described as the minimization of the following unidirectional variation model:

$$\min_u \|\nabla_x(u - g)\|_1 + \lambda \|\nabla_y u\|_1 \quad (2)$$

where $\|\nabla_x(u - g)\|_1$ is called data item, which is used to ensure that the difference between the results constructed and the original image will not be too large. The term $\|\nabla_y u\|$ denotes the horizontal and vertical variations of the image u , which is used to eliminate the image's stripe noise of. $\lambda > 0$ is the regularization parameter. If λ is very small, the noise cannot be removed well. If λ is very large, the detailed information included edge will be blurred. Therefore, the parameter λ should be chosen the appropriate value to ensure the best results according to the noise.

Although this model can effectively eliminate the stripe noise, it's still easy to cause the "ripple phenomenon" in the flat area of the image. But in the flat area, it is still easy to cause the "ripple phenomenon". To eliminate the "ripple phenomenon", we propose the following higher-order algorithm model:

$$\min_u \|\nabla_{xx}(u - g)\|_1 + \lambda \|\nabla_{yy} u\|_1 \quad (3)$$

In formula (3), ∇_{xx} is higher-order differential operator in X -direction and ∇_{yy} is higher-order differential operator in Y -direction.

3. Optimization Problem Solution

The higher-order differential equation contains the l_1 term, which is no differentiability. It is difficult in solutions by using traditional numerical method. Then, we used the Split-Bregman method to solve this problem. The Split-Bregman method is a very efficient method to solve the l_1 -regularized optimization problems in [11]. The Split-Bregman method's principle is that the original problem is converted to several sub-problems by introducing the relevant auxiliary variables, so that the problem becomes smaller, and it can be easily solved. Set $d_x = \nabla_{xx}(u - g)$, $d_y = \nabla_{yy}u$, the original problem (3) leads to a constrained optimization problem as follows:

$$\begin{cases} \min_{u, d_x, d_y} \|d_x\|_1 + \lambda \|d_y\|_1 \\ \text{s.t. } d_x \nabla_{xx}(u - g), d_y = \nabla_{yy}u \end{cases} \quad (4)$$

Formula (4) can be approximated by adding two penalty function terms. It is an unconstrained problem as follows:

$$\begin{aligned} & \min_{u, d_x, d_y} \|d_x\|_1 + \lambda \|d_y\|_1 + \frac{\alpha}{2} \|d_x - \nabla_{xx}(u - g)\|_2^2 \\ & + \frac{\beta}{2} \|d_y - \nabla_{yy}u\|_2^2 \end{aligned} \quad (5)$$

In formula (5), α and β are both penalty parameters. The constraints are strictly enforced by applying the Bregman iteration, and then there are three sub-problems as follows:

$$\begin{aligned} & \min_{u, d_x, d_y} \|d_x\|_1 + \lambda \|d_y\|_1 + \frac{\alpha}{2} \|d_x - \nabla_{xx}(u - g) - b_x\|_2^2 \\ & + \frac{\beta}{2} \|d_y - \nabla_{yy}u - b_y\|_2^2 \end{aligned} \quad (6)$$

$$b_x^{k+1} = b_x^k + \nabla_{xx}(u^{k+1} - g) - d_x^{k+1} \quad (7)$$

$$b_y^{k+1} = b_y^k + \nabla_{yy}u^{k+1} - d_y^{k+1} \quad (8)$$

We can simplify the three sub-problems even further through the first sub-problem is split into solution of u , d_x and d_y , thus the problem can be solved as follows:

$$\min_u \frac{\alpha}{2} \|d_x^k - \nabla_{xx}(u - g) - b_x^k\|_2^2 + \frac{\beta}{2} \|d_y^k - \nabla_{yy}u - b_y^k\|_2^2$$

$$\min_{d_x} \|d_x\|_1 + \frac{\alpha}{2} \|d_x - \nabla_{xx}(u^{k+1} - g) - b_x^k\|_2^2$$

$$\min_{d_y} \lambda \|d_y\|_1 + \frac{\beta}{2} \|d_y - \nabla_{yy}u^{k+1} - b_y^k\|_2^2 \quad (9)$$

$$b_x^{k+1} = b_x^k + \nabla_{xx}(u^{k+1} - g) - d_x^{k+1}$$

$$b_y^{k+1} = b_y^k + \nabla_{yy}u^{k+1} - d_y^{k+1}$$

Then, we investigate the above sub-problems one by one:

(1) u sub-problem. Note that Step 1 is a higher-order function minimization problem. Therefore, the problem can be solved as follows:

$$\begin{aligned} & \alpha \nabla_{xx}^T \nabla_{xx}(u^{k+1} - g) + \beta \nabla_{yy}^T \nabla_{yy}u^{k+1} = \alpha \nabla_{xx}^T (d_x^k - b_x^k) \\ & + \beta \nabla_{yy}^T (d_y^k - b_y^k) \end{aligned} \quad (10)$$

Due to $\nabla_x^T = -\nabla_x$, $\nabla_{xx}^T = \nabla_{xx}$, $\nabla_{yy}^T = \nabla_{yy}$, formula (10) can be simplified as follows:

$$\begin{aligned} & (\alpha \nabla_{xx} \nabla_{xx} + \beta \nabla_{yy} \nabla_{yy})u^{k+1} = \alpha \nabla_{xx}(d_x^k - b_x^k) \\ & + \beta \nabla_{yy}(d_y^k - b_y^k) + \alpha \nabla_{xx} \nabla_{xx}g \end{aligned} \quad (11)$$

Because of formula (11) being strictly diagonal, the local differential operators ∇_{xx} , $\nabla_{xx} \nabla_{xx}$, ∇_{yy} and $\nabla_{yy} \nabla_{yy}$ are as follows:

$$\begin{aligned} \nabla_{xx} \nabla_{xx} u &= u_{i+2,j} - 4u_{i+1,j} + 6u_{i,j} - 4u_{i-1,j} + u_{i-2,j} \\ \nabla_{xx} u &= u_{i+1,j} + u_{i-1,j} - 2u_{i,j} \\ \nabla_{yy} \nabla_{yy} u &= u_{i,j+2} - 4u_{i,j+1} + 6u_{i,j} - 4u_{i,j-1} + u_{i,j-2} \\ \nabla_{yy} u &= u_{i,j+1} + u_{i,j-1} - 2u_{i,j} \end{aligned} \quad (12)$$

By merging similar terms, we can obtain following the update formula of image u :

$$\begin{aligned}
u_{i,j}^{k+1} = & \frac{\alpha}{6\alpha + 6\beta} (4u_{i+1,j}^k + 4u_{i-1,j}^k - u_{i-2,j}^k - u_{i+2,j}^k) \\
& + \frac{\beta}{6\alpha + 6\beta} (4u_{i,j+1}^k + 4u_{i,j-1}^k - u_{i,j-2}^k - u_{i,j+2}^k) \\
& + \frac{\alpha}{6\alpha + 6\beta} (d_{x,i+1,j}^k + d_{x,i-1,j}^k - 2d_{x,i,j}^k - b_{x,i+1,j}^k \\
& - b_{x,i-1,j}^k + 2b_{x,i,j}^k) \\
& + \frac{\beta}{6\alpha + 6\beta} (d_{y,i,j+1}^k + d_{y,i,j-1}^k - 2d_{y,i,j}^k - b_{y,i,j+1}^k \\
& - b_{y,i,j-1}^k + 2b_{y,i,j}^k) \\
& + \frac{\alpha}{6\alpha + 6\beta} (g_{i+2,j} - 4g_{i+1,j} + 6g_{i,j} - 4g_{i-1,j} \\
& + g_{i-2,j})
\end{aligned} \tag{13}$$

(2) We compute dx , dy by using the following formula from [12].

$$d_x^{k+1} = \text{shrink} \left(\nabla_{xx} (u^{k+1} - g) + b_x^k, \frac{1}{\alpha} \right) \tag{14}$$

$$d_y^{k+1} = \text{shrink} \left(\nabla_{yy} u^{k+1} + b_y^k, \frac{\lambda}{\beta} \right) \tag{15}$$

where

$$\text{shrink}(r, \xi) = \frac{r}{|r|} \max(|r| - \xi, 0) \tag{16}$$

The complete procedure of the destriping noise is summarized as Algorithm 1.

Algorithm 1: Higher-order unidirectional total variation with HOUTV-SBI

1. **Initialization:** $u^0 = g$, $d_x^0 = d_y^0 = b_x^0 = b_y^0 = 0$, $k = 0$, $n_{\max} = 80$.
2. **While** $\|u^k - u^{k-1}\|_2 / \|u^k\|_2 > \varepsilon$ and $k < n_{\max}$, **do**
3. **Update** u^{k+1} by using formula (13);
4. **Solve** $d_x^{k+1} = \text{shrink} \left(\nabla_{xx} (u^{k+1} - g) + b_x^k, \frac{1}{\alpha} \right)$;
5. **Solve** $d_y^{k+1} = \text{shrink} \left(\nabla_{yy} u^{k+1} + b_y^k, \frac{\lambda}{\beta} \right)$;
6. **Solve** $b_x^{k+1} = b_x^k + \nabla_{xx} (u^{k+1} - g) - d_x^{k+1}$;
7. **Solve** $b_y^{k+1} = b_y^k + \nabla_{yy} u^{k+1} - d_y^{k+1}$;
8. $k = k + 1$
9. **End While**

4. Experimental Results

In experiments, two types of RS images are affected from the stripe noise in Fig. 1. The first category is the hyperspectral data from EO1 satellite images shown in Fig. 1(a). The other data comes from MODIS satellite

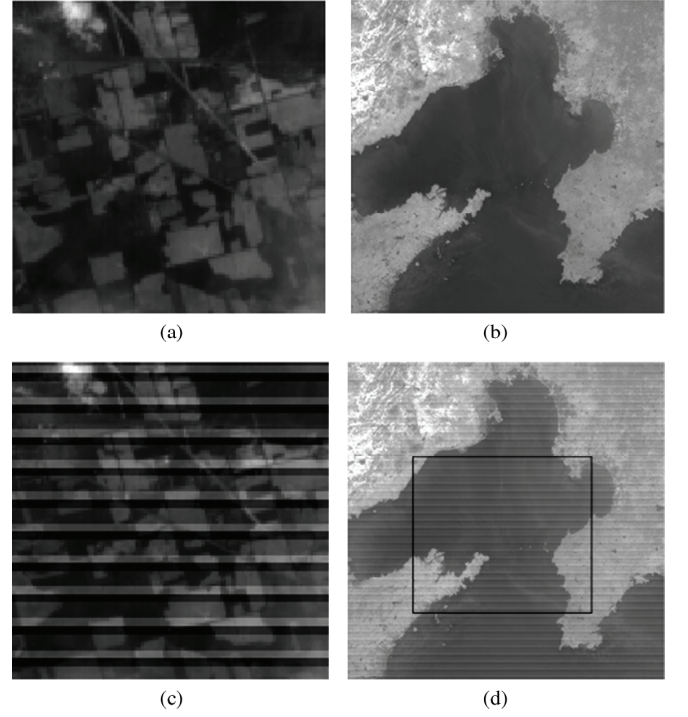


Figure 1. The test image: (a) The original image from hyperspectral; (b) The original image from MODIS; (c) The stripe noise of the hyperspectral image; and (d) the stripe noise of MODIS image.

images shown in (b). The degraded results of the two types of images are shown in Fig. 1(c) and (d).

To show the performance of our proposed method, we compare the performance against the three representative algorithms on removing stripe in the experiment. The tested algorithms are Wavelet-fast fourier transform (FFT) [13], statistical linear destriping (SLD) [14], and UTV-SBI [7]. We use peak signal to noise ratio (PSNR) [15] to measure the improve effect of image destriping with the ground-truth images. In Table 1, there shows the values of the four methods in PSNR.

From Table 1, compared to the other methods, the HOUTV-SBI has the best performance of the highest PSNR value For UTV-SBI and HOUTV-SBI methods, we make the penalization parameters $\alpha = \beta = 1$, the regularization parameter $\lambda = 0.0250, 0.0275, 0.030, \dots, 0.2500$ and the maximum number of iterations $n_{\max} = 300$. In Wavelet-FFT method, the parameters are set as: decomposition level L from 1 to 8, wavelet type W from DB1 to DB42, and damping factor σ from 1 to 16. The parameters of the SLD [13] method are set as: $\lambda = 0.01, 0.05, 0.1, 0.5, 1$, and $s = 10^0, 10^1, \dots, 10^5$. We take the above parameter space traversed for all methods and choose the highest PSNR.

To verify the effectiveness of removing strip of each method further, the destriped results in the highest PSNR are shown in Fig. 2.

From Table 1 and Fig. 2, it shows that the PSNR of UTV-SBI is higher than that of Wavelet-FFT, so UTV-SBI method gives a better effect for RS images.

Table 1
PSNR Comparisons

Methods		Original	Wavelet-FFT	SLD	UTV-SBI	Our Method (HOUTV-SBI)
RS images	Fig. 1(a)	18.59	30.65	19.52	31.32	31.54
	Fig. 1(b)	32.44	41.45	41.78	41.48	42.12

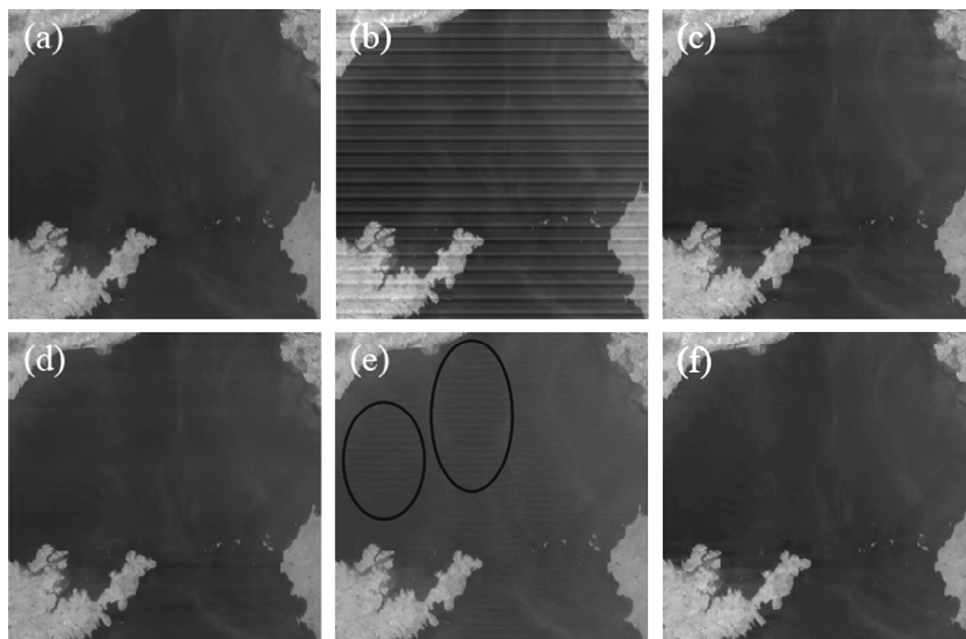


Figure 2. The results of destriping in different methods: (a) Fig. 1(b) Zoom; (b) The stripe noise; (c) The result of Wavelet-FFT ($L = 4$, $W = \text{DB2}$, $\sigma = 3$); (d) The result of SLD ($\lambda = 1$, $s = 1$); (e) The result of UTV-SBI ($\lambda = 0.0275$); and (f) the result of HOUTV-SBI ($\lambda = 0.0250$).

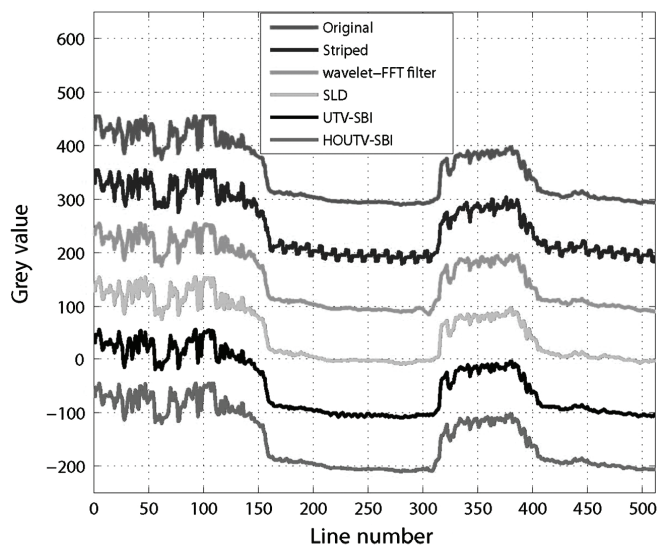


Figure 3. The results of destriping in 128th column.

Table 2
ID Comparisons of the Four Methods

Image	Wavelet-FFT	SLD	UTV-SBI	HOUTV-SBI
Fig. 1(a)	0.566	0.587	0.597	0.629
Fig. 1(b)	0.828	0.846	0.852	0.875

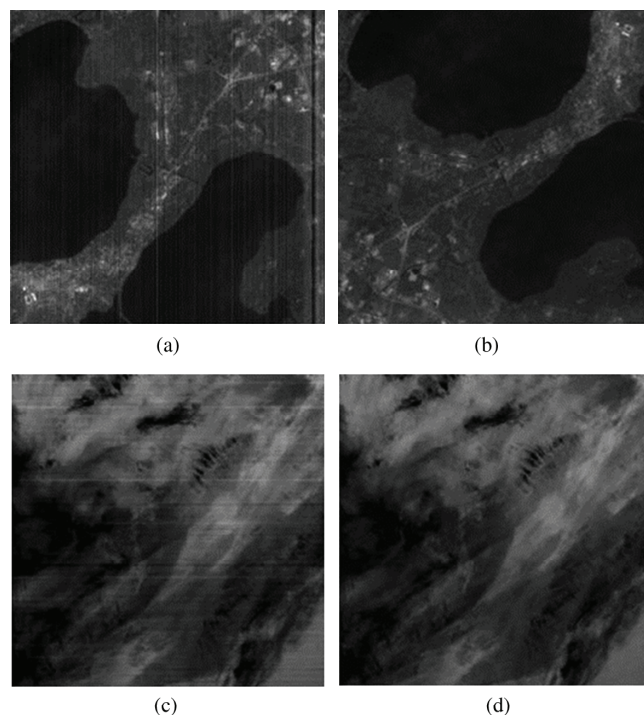


Figure 4. The destriping results in proposed method: (a) The original hyperspectral image (band = 136); (b) The result of destriping ($\lambda = 0.0250$); (c) The original image from MODIS (band = 35) and (d) the result of destriping ($\lambda = 0.0250$).

The Wavelet-FFT and SLD methods also have a few of residual strips in the image. In Fig. 3, we compare the de-striping effect in the 128th column of the stripe noise. The results of de-striping in 128th column reveal that HOUTV-SBI method has a better effect than the other methods.

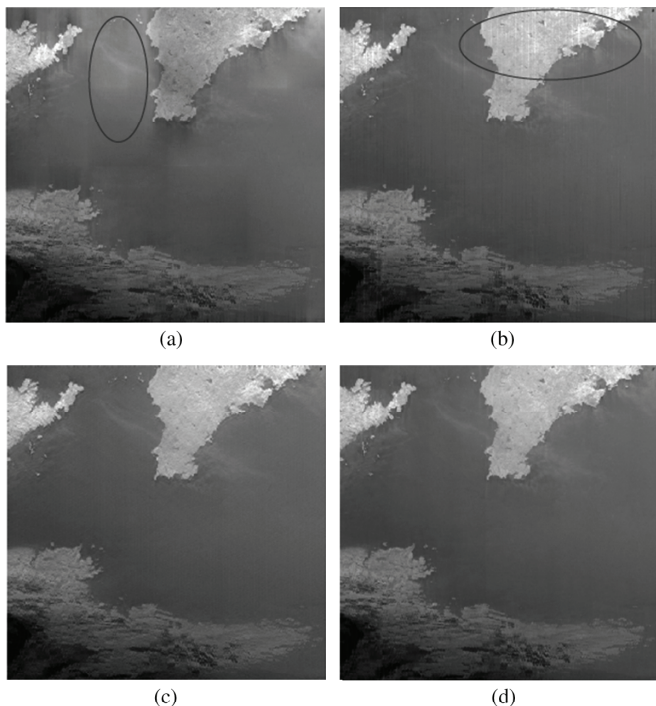


Figure 5. The results of de-striping in agricultural monitoring satellite images: (a) Wavelet-FFT; (b) SLD; (c) UTV-SBI; and (d) HOUTV-SBI.

To measure the effect of our method more fully, we also use the image distortion (ID) index. The high ID values means has a smaller distortion. The ID values for the four methods are shown in Table 2. From Table 2, it shows that HOUTV-SBI has also the best performance with the smallest distortion in all methods.

Our method still can get a good effect of removing strip in other images as shown in Fig. 4.

To test the universality of our method for the agricultural RS images, we choose the farmland water conservancy monitoring satellite images in experiments. Our proposed method is also compared with Wavelet-FFT, SLD, and UTV-SBI. The results of de-striping are shown in Fig. 5.

From Fig. 5, it can be seen that wavelet-FFT can remove the band of the image, but the grey values have been significantly deviated from those of the original image, the grey values are brighter than those of the original image. SLD and wavelet-FFT appear more stripe residues in the red ellipse areas. Compared with other two methods, UTV-SBI and HOUTV-SBI can remove the stripe noise better. Figure 6 is their power spectrum. It can be found that the column power spectrum has the abrupt changes at frequencies (0.1, 0.2, 0.3, 0.4, 0.5) in the original image. And the column power spectrum has a little with residua at frequencies (0.4, 0.2) in the images destriped by Wavelet-FFT filter and UTV-SBI, while it has a significant remnant at frequencies (0.3, 0.4) by SLD. However, the curve of the column power spectrum is smooth by HOUTV-SBI. From the above results, it can be seen that our proposed method takes the best effect on removing the stripe noises of the agricultural monitoring images.

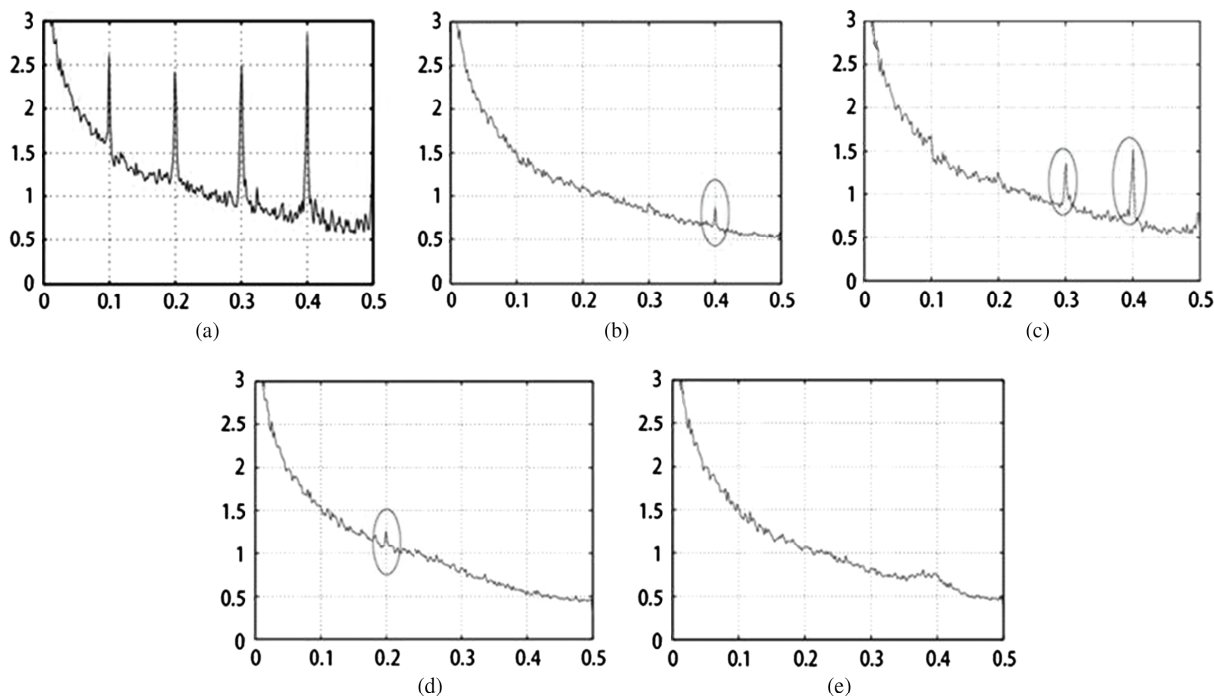


Figure 6. The power spectra of destriped images: (a) The original image; (b) By Wavelet-FFT; (c) By SLD; (d) By UTV-SBI; and (e) by HOUTV-SBI.

5. Conclusion

Focusing on the problem of removing the strip noise in agricultural RS images, we proposed a novel kind of higher-order partial differential algorithm model to removing stripe in this paper, and used the Split-Bregman iterative method to solve quickly. Through experiments to destriping in real Hyperspectral, MODIS satellite images and simulation images, it can be seen that our proposed method could effectively remove the stripe noises in RS images and not cause the “ripple phenomenon”. The effect of our method with the higher-order model is much better than the lower-order model. Moreover, our method becomes more robust and has a good effect on agricultural monitoring.

Acknowledgement

The work was sponsored by the Research Fund for Excellent Dissertation of China Three Gorges University and the Project of the HuBei Foundation for Innovative Research Groups (Grant no. 2015CFA025).

References

- [1] R. Chinniah and S.S. Rani, A sparse based rain removal algorithm for image sequences, *International Journal of Robotics and Automation*, 29(4), 2014, 4086–4088.
- [2] L.L. Guo, Z.P. Wu, L.G. Zhang, *et al.*, Destriping of remote sensing images with applications to push-broom-type cameras, *Journal of Optics*, 33(8), 2013, 0828001.1-07.
- [3] S. Niu, J. Tang, X. Jiang, *et al.*, The comparison of two quantitative striping removal algorithms for HY-1A COCTS data, *Journal of Remote Sensing*, 11(6), 2007, 860–867.
- [4] F.L. Gadallah and F. Csillag, Destriping multi-detector imagery with moment matching, *International Journal of Remote Sensing*, 21(12), 2000, 2505–2511.
- [5] J.G. Liu and K. Morgan, FFT selective and adaptive filtering for removal of systematic noise in ETM+ Imageodesy images, *IEEE Transactions on Geoscience and Remote Sensing*, 44(12), 2006, 3716–3724.
- [6] J. Torres and S. Infantes, Wavelet analysis for the elimination of striping noise in satellite images. *Optical Engineering*, 40(7), 2001, 1309–1314.
- [7] M. Bouali and S. Ladjal, Toward optimal destriping of MODIS data using a unidirectional variational model, *IEEE Transactions on Geoscience and Remote Sensing*, 49(8), 2011, 2924–2935.
- [8] R. Pande-Chhetri and A. Abd-Elrahman, De-striping hyperspectral imagery using wavelet transform and adaptive frequency domain filtering, *ISPRS Journal of Photogrammetry & Remote Sensing*, 66(5), 2011, 620–636.
- [9] H. Shen and L. Zhang, A MAP-based algorithm for destriping and inpainting of remotely sensed images, *IEEE Transactions on Geoscience and Remote Sensing*, 47(5), 2009, 1492–1502.
- [10] H. Gan, N. Sang, and R. Huang, Manifold regularized semi-supervised Gaussian mixture model, *Journal of the Optical Society of America A*, 32, 2015, 566–575.
- [11] T. Goldstein and S. Osher, The split Bregman method for L1-regularized problems. *SIAM Journal on Imaging Sciences*, 2(2), 2009, 323–343.
- [12] Y. Wang, J. Yang, W. Yin, and Y. Zhang, A new alternating minimization algorithm for total variation image construction, *SIAM Journal on Imaging Sciences*, 1(3), 2008, 248–272.
- [13] B. Munch, P. Trtik, F. Marone, and M. Stampanoni, Stripe and ring artifact removal with combined wavelet–Fourier filtering, *Optics Express*, 17(10), 2009, 8567–8591.
- [14] H. Carfantan and J. Idier, Statistical linear destriping of satellite-based pushbroomtype images, *IEEE Transactions on Geoscience and Remote Sensing*, 48(4), 2010, 1860–1871.

- [15] L. Yan, M. Jin, H. Fang, *et al.*, Atmospheric-turbulence-degraded astronomical image restoration by minimizing second-order central moment, *IEEE Geoscience & Remote Sensing Letters*, 9(4), 2012, 672–676.

Biographies



Zhiping Dan received his B.S. degree from the Mathematics Department, Wuhan University, China, in 1997, and the M.S. degree from the Mathematics Department, Huazhong University of Science and Technology, China, in 2005. He received his Ph.D. degree from the Institute for Pattern Recognition and Artificial Intelligence, Huazhong University of Science and Technology, China, in 2013. He is currently a professor in the College of Computer and Information Technology, China Three Gorges University. His research interests are in the areas of computer vision, image processing, and machine learning.

Zhiping Dan received his B.S. degree from the Mathematics Department, Wuhan University, China, in 1997, and the M.S. degree from the Mathematics Department, Huazhong University of Science and Technology, China, in 2005. He received his Ph.D. degree from the Institute for Pattern Recognition and Artificial Intelligence, Huazhong University of Science and Technology,



Xing Wei received his B.S. degree from Wuchang Shouyi University in 2014. Currently he is a graduate student at China Three Gorges University. His research interests mainly include image processing and multiple target tracking.



Shuifa Sun received two B.S. degrees in application physics and in radio technique, respectively, from Tianjin University, Tianjin, China, in 1999, the M.S. degree in telecommunication and information system from Zhejiang University of Technology, in 2002, and Ph.D. degree in information and telecommunication engineering from Zhejiang University in 2005. From May 2005 to April 2006, he was a research associate at the Department of Computer Science, City university of Hong Kong. From May 2006 to August 2006, he was a post-doctoral research fellow at the Research Institute of Information Technology, Tsinghua University, Beijing, China. Since August 2006, he has been with China Three Gorges University, Yichang, Hubei, China, where he is now a full professor. His research interests include computer vision, biomedical image processing, three-dimensional modelling and visualization, information security. He is a member of the IEEE Signal Processing Society and ACM.

Shuifa Sun received two B.S. degrees in application physics and in radio technique, respectively, from Tianjin University, Tianjin, China, in 1999, the M.S. degree in telecommunication and information system from Zhejiang University of Technology, in 2002, and Ph.D. degree in information and telecommunication engineering from Zhejiang University in 2005. From May 2005 to April



Gang Zhou graduated from the Changsha University of Science and Technology and received his B.S. degree in 2006. He received his M.S. degree in statistic and signals process from Guizhou Nationalities University in 2010 and obtained a Ph.D. degree in 2016 from the Institute for Pattern Recognition and Artificial Intelligence, Huazhong University of Science and Technology, Wuhan,

China. Now, he is a research fellow in HUST. His main researches include superresolution, moving detection, and pattern recognition.